JOURNAL OF IRON AND STEEL RESEARCH, INTERNATIONAL. 2015, 22(9): 827-836

Hot Deformation Behavior and Flow Stress Prediction of Ultra Purified 17% Cr Ferritic Stainless Steel Stabilized with Nb and Ti

Fei GAO[1], Fu-xiao YU[1], Hai-tao LIU[2], Zhen-yu LIU[2]
(1. School of Materials & Metallurgy, Northeastern Unversity, Shenyang 110819, Liaoning, China; 2. State Key Laboratory of Rolling and Automation, Northeastern University, Shenyang 110819, Liaoning, China)

Abstract: The hot deformation behavior of ultra purified 17% Cr ferritic stainless steel stabilized with Nb and Ti was investigated using axisymmetric hot compression tests on a thermomechanical simulator. The deformation was carried out at the temperatures ranging from 700 to 1 100 ℃ and strain rates from 1 to 10 s^{-1}. The microstructure was investigated using electron backscattering diffraction. The effects of temperature and strain rate on deformation behavior were represented by Zener-Hollomon parameter in an exponent type equation. The effect of strain was incorporated in the constitutive equation by establishing polynomial relationship between the material constants and strain. A sixth order polynomial was suitable to represent the effect of strain. The modified constitutive equation considering the effect of strain was developed and could predict the flow stress throughout the deformation conditions except at 800 ℃ in 1 s^{-1} and at 700 ℃ in 5 and 10 s^{-1}. Losing the reliability of the modified constitutive equation was possibly ascribed to the increase in average Taylor factor at 800 ℃ in 1 s^{-1} and the increase in temperature at 700 ℃ in 5 and 10 s^{-1} during hot deformation. The optimum window for improving product quality of the ferritic stainless steels was identified as hot rolling at a low finisher entry temperature of 700 ℃, which can be achieved in practical production.
Key words: 17%Cr ferritic stainless steel; hot deformation; flow stress; constitutive equation; strain compensation

In recent years, the stainless steel market has been characterized by an increased application of ferritic grades at the expense of Cr-Ni austenitic grades because ferritic grades have higher yield strength, superior stress corrosion cracking resistance and lower cost compared with Cr-Ni austenitic grades[1-6]. However, ferritic stainless steels possess poor formability and surface quality in comparison with austenitic stainless steels, which can be attributed to low r-value, severe surface ridging and sticking phenomenon during hot rolling of the ferritic stainless steel[1,7], and thus the extensive applications of the ferritic stainless steels may be restricted.

The way to improve formability and surface quality of final sheet for the ferritic stainless steels is to increase the r-value, enhance the ridging resistance and prevent the sticking, which can be attempted by controlling hot rolling and optimizing hot rolling schedule[4,5,7-12]. Nevertheless, in order to carry out the improved hot rolling process smoothly, determining the load is important. Load is closely related to the flow stress of the materials. Therefore, the understanding of hot deformation behavior and establishing a constitutive equation, which can accurately predict the flow stress, are important in controlling the hot rolling process and improving the product quality of the ferritic stainless steels.

In the past, many efforts have been devoted to understand the hot deformation behavior and predict the flow stress of the ferritic stainless steels, such as 409L ferritic stainless steel[13], 430 ferritic stainless steel (0.028% C, 16.355% Cr)[14], high purified 17% Cr ferritic stainless steel[15], and ultra purified 21% Cr ferritic stainless steel[16]. In most studies, however, constitutive equations were based on the Arrhenius type equation and the assumption that the effect of strain on hot deformation behavior is insignificant. In fact, the effect of strain is significant, especially at relatively low deformation tem-

Foundation Item: Item Sponsored by National Science and Technology Pillar Program during the Twelfth Five-year Plan Period of China (2012BAE04B02); National Natural Science Foundation of China (51271050)
Biography: Fei GAO, Doctor Candidate; **E-mail**: gaofei181@aliyun.com; **Received Date**: May 19, 2014

peratures. For including strain effects, the strain-dependent constants were determined and incorporated into the constitutive equation by Slooff et al.[17,18], which led to the accurate prediction of flow stress in a wrought magnesium alloy. This method was later used successfully for austenitic stainless steels[19,20], martensitic precipitation hardening stainless steels[20], carbon steels[21,22] and other alloys[23,24]. So far, little systematic work has been carried out on establishing the constitutive equation describing the flow stress as a function of strain, strain rate and temperature for ultra purified 17% Cr ferritic stainless steel with the final aims of clarifying the optimum hot rolling process parameters and improving the final product quality, and analyzing the reliability and stability of corresponding constitutive equation in detail.

In this work, the hot deformation behavior of ultra purified 17% Cr ferritic stainless steel stabilized with Nb and Ti was investigated with hot compression tests on a thermo-mechanical simulator. The microstructure was investigated using electron backscattering diffraction (EBSD). The flow stress curve was employed to develop constitutive equation. The modified constitutive equation was developed by considering the effect of strain on material constants, and the reliability of developed constitutive equation was also analyzed in depth. Finally, the optimum hot rolling window was clarified for improving product quality of the ferritic stainless steels and its feasibility was analyzed.

1 Experimental Procedure

The chemical compositions in mass percent of ultra purified 17% Cr ferritic stainless steel stabilized with Nb and Ti, which was prepared by vacuum melting and casting in the laboratory, are C 0.006%, N 0.006%, Ti 0.14%, Nb 0.06%, Cr 17.2%, V 0.11%, Si 0.19%, Mn 0.25% and Fe balance. The experimental steel was heated at 1 200 ℃ for 1 h and then hot rolled to 12 mm thick hot band in the temperature range from 980 ℃ to 1 100 ℃. Cylindrical specimens with diameter of 8 mm and length of 15 mm were machined with their axes parallel to the rolling direction of the hot band. Hot deformation was performed using isothermal hot compression tests on a thermo-mechanical simulator. As shown in Fig. 1, the specimens were heated to 1 200 ℃ at a heating rate of 20 ℃ · s^{-1}, held for 180 s to homogenize the microstructure and cooled to deformation temperatures ranging from 700 to 1 100 ℃ at a cooling rate of 10 ℃ · s^{-1}. The specimens were also held for 30 s to eliminate a thermal gradient. Then, the specimens were deformed at strain rates of 1 to 10 s^{-1} to the strain ε of 0.6. After deformation, the specimens were immediately water quenched in situ. One cylindrical specimen was water quenched after 180 s of homogenization treatment at 1 200 ℃ in order to analyze the initial microstructure before deformation.

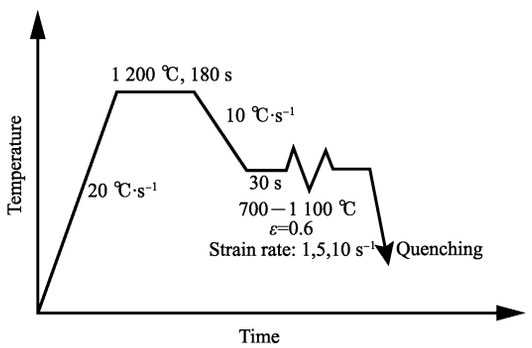

Fig. 1 Schematic illustration of hot compression tests

Microstructure analyses were performed using EBSD. The samples for EBSD measurement were prepared by electrolytic polishing in 50 mL $HClO_4$ + 100 mL H_2O + 650 mL C_2H_5OH. The data obtained from the EBSD measurement were post-processed using HKL Channel 5 flamenco software. It is noted that cross-sections of cylindrical compression specimens halved parallel to the cylinder axis were used for the microstructure analyses.

2 Results and Discussion

Fig. 2 shows the flow stress curves of experimental steel during hot deformation. It is clearly shown that the flow stress curves under different deformation conditions possess similar shape, which resembles that of flow stress curves previously observed for other ferritic stainless steels[16,25]. The flow stress curves typically show a work hardening region followed by dynamic softening due to recovery and/or recrystallization.

From Fig. 2, it can also be seen that the deformation temperature and strain rate have significant effect on the flow stress. The flow stress decreases with increasing deformation temperature and decreasing strain rate. This is due to the fact that higher temperatures and lower strain rates offer higher mobilities of dislocation and grain boundary and longer time can benefit the annihilation and rearrangement of dislocations and the formation and coalescence of subgrains.

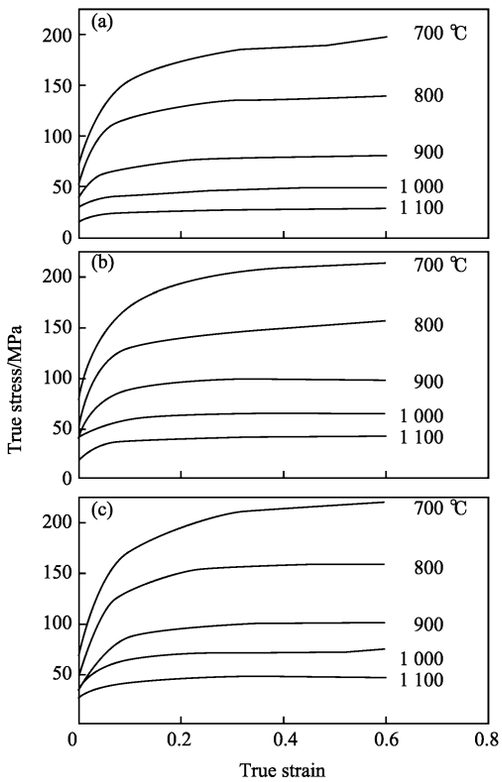

(a) 1 s^{-1}; (b) 5 s^{-1}; (c) 10 s^{-1}.

Fig. 2 Flow stress curves of experimental steel at 700—1 100 ℃ and different strain rates

In addition, the effect of strain rate on flow stress is closely related to the deformation temperature. The strain rate sensitivity is an important parameter for evaluating the sensitivity of the flow stress to strain rate during the plastic deformation, which reflects the work hardening tendency with increasing strain rate. The effect of strain rate on flow stress is enhanced, that is, the strain rate sensitivity increases when the deformation temperature increases (Fig. 2). This can be ascribed to increasing elimination rate of work hardening with increasing deformation temperature[26,27].

The change of flow stress increases with increasing softening amount. The amount of softening can be determined by the elimination rate and time of work hardening. The amount of softening increases with increasing elimination rate and hardening time. On one hand, the elimination rate of work hardening is related to deformation temperature and strain. The elimination rate of work hardening increases with increasing deformation temperature and strain. At constant strain, hence, when deformation temperature increases, the elimination rate of work hardening increases, resulting in increasing softening amount. On the other hand, the elimination time of work hardening is related to strain rate. The elimination time of work hardening increases with decreasing strain rate. At constant strain rate, hence, the elimination time of work hardening and the amount of softening are invariable. Therefore, when the decrease of strain rate is a constant, the amount of softening at the high deformation temperature is higher than that at low deformation temperature at constant strain. That is, the effect of strain rate on the amount of softening enhances when the deformation temperature increases.

2.1 Constitutive equations for flow stress prediction

It is well known that hot deformation can be considered as a thermally activated process and is similar to the creep phenomenon. Various constitutive equations similar to those employed in creep studies are developed to model the hot deformation behavior, and these equations can be expressed as follows[19-21,28-31]:

$$\dot{\varepsilon} = A_1\sigma^{n_1} \cdot \exp\left(-\frac{Q}{RT}\right) \quad (\text{for low stress level}, \alpha\sigma < 0.8) \tag{1}$$

$$\dot{\varepsilon} = A_2\exp(\beta\sigma) \cdot \exp\left(-\frac{Q}{RT}\right) \quad (\text{for high stress level}, \alpha\sigma > 1.2) \tag{2}$$

$$\dot{\varepsilon} = A\left[\sinh(\alpha\sigma)\right]^n \cdot \exp\left(-\frac{Q}{RT}\right) \quad (\text{for all stress level}) \tag{3}$$

where, A_1, n_1, A_2, β, A, α and n are the material constants; α ($\approx\beta/n_1$) is the stress multiplier, MPa^{-1}; Q is the activation energy of hot deformation, $kJ \cdot mol^{-1}$; R is the gas constant, 8.314 5 $J \cdot mol^{-1} \cdot K^{-1}$; $\dot{\varepsilon}$ is the strain rate, s^{-1}; σ is the flow stress for a given strain, MPa; and T is the deformation temperature, K.

For low stress level, Eq. (1) is used to describe the hot deformation behavior. For high stress level, Eq. (2) is used. For all stress level, Eq. (3) can be applied. When the stress level is low, i.e., $\sinh(\alpha\sigma)\approx\alpha\sigma$, Eq. (3) can be simplified as Eq. (1) and A_1 and n_1 are $A\alpha^n$ and n, respectively. When the stress level is high, i.e., $\sinh(\alpha\sigma)\approx 0.5\exp(\alpha\sigma)$, Eq. (3) can be simplified as Eq. (2) and A_2 and β are $A/2^n$ and $n\alpha$, respectively.

In addition, the effects of temperature and strain rate on hot deformation behavior can be described by the Zener-Holloman parameter Z in an exponent type equation, and this equation can be expressed as follows[32]:

$$Z = \dot{\varepsilon} \cdot \exp(\frac{Q}{RT}) \tag{4}$$

2.2 Determination of strain-dependent material constants

It is commonly accepted that constitutive equations (Eqs. (1), (2) and (3)) are based on the assumption that the effect of strain on hot deformation behavior is insignificant. In fact, the effect of strain is significant, especially at relatively low deformation temperatures. At each value of strain, the flow stress curves are in different deformation stages and exhibit different deformation or softening mechanisms. As a result, the effect of strain should be taken into account in order to derive a constitutive equation that accurately predicts the flow stress. In this study, in order to compensate the strain, the material constants for the constitutive equation were determined at different strains and the effect of strain on the material constants was incorporated in the constitutive equation by assuming that the material constants are a polynomial function of the strain. Taking the strain of 0.25 as an example, the solution procedure of material constants was conducted.

Taking natural logarithm of both sides of Eqs. (1) and (2) gives

$$\ln\dot{\varepsilon} = \ln A_1 + n_1 \ln\sigma - \frac{Q}{RT}$$
(for low stress level) (5)

$$\ln\dot{\varepsilon} = \ln A_2 + \beta\sigma - \frac{Q}{RT}$$
(for high stress level) (6)

From Eq. (5), it can be seen that an optimum n_1 can be obtained by plotting $\ln\dot{\varepsilon}$ against $\ln\sigma$ at constant temperature, and the mean value of the reciprocals of the slopes of the lines in the $\ln\sigma$-$\ln\dot{\varepsilon}$ plot gives the value of n_1. From Eq. (6), it can be seen that an optimum β value can be obtained by plotting $\ln\dot{\varepsilon}$ against σ at constant temperature, and the mean value of the reciprocals of the slopes of the lines in the σ-$\ln\dot{\varepsilon}$ plot gives the value of β. Using the values of the flow stress and corresponding strain rate at 0.25 strain, the values of n_1 and β were found to be 10.072 and 0.100 MPa^{-1} by establishing the relationship between $\ln\sigma$ and $\ln\dot{\varepsilon}$ and relationship between σ and $\ln\dot{\varepsilon}$, respectively. Then, α is 0.009 9 MPa^{-1}.

Taking natural logarithm of both sides of Eq. (3) gives

$$\ln\dot{\varepsilon} = \ln A + n\ln[\sinh(\alpha\sigma)] - \frac{Q}{RT}$$
(for all stress level) (7)

After partial differentiation of Eq. (7) and some algebraic operations, following equation can be obtained:

$$Q = R \cdot \left.\frac{\partial \ln\dot{\varepsilon}}{\partial \ln[\sinh(\alpha\sigma)]}\right|_T \cdot \left.\frac{\partial \ln[\sinh(\alpha\sigma)]}{\partial (1/T)}\right|_{\dot{\varepsilon}} \tag{8}$$

From Eq. (8), it can be seen that the value of Q can be obtained from the mean value of the reciprocals of the slopes of the lines in the $\ln[\sinh(\alpha\sigma)]$-$\ln\dot{\varepsilon}$ plot and the mean value of the slopes of the lines in the $\ln[\sinh(\alpha\sigma)]-1/T$ plot. With the values of the flow stress, deformation temperature and corresponding strain rate at 0.25 strain, the relationship between $\ln[\sinh(\alpha\sigma)]$ and $\ln\dot{\varepsilon}$ and relationship between $\ln[\sinh(\alpha\sigma)]$ and $1\,000/T$ can be obtained, as shown in Fig. 3, and the value of Q is 424 352.803 $J \cdot mol^{-1}$. Then, by substituting the values of Q, $\dot{\varepsilon}$ and T into Eq. (4), the values of Z can be obtained at different deformation temperatures and strain rates.

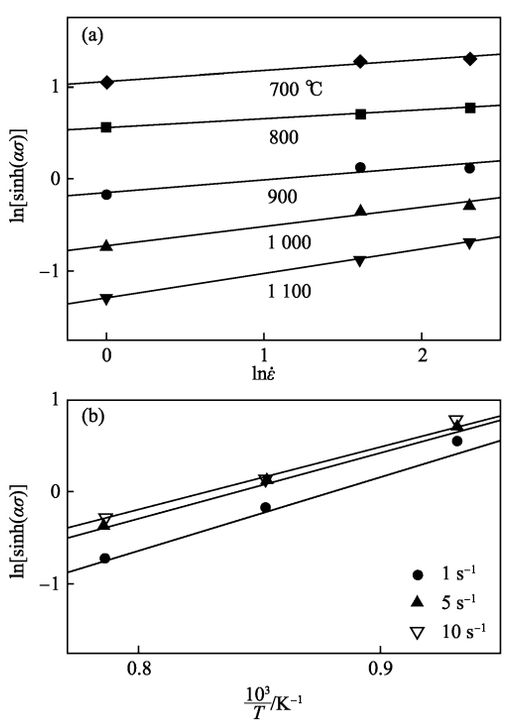

Fig. 3 Relationship of $\ln[\sinh(\alpha\sigma)]$ to $\ln\dot{\varepsilon}$ and $\ln[\sinh(\alpha\sigma)]-1\,000/T$ for the experimental steel

From Eqs. (3) and (4), following equation can be obtained

$$Z = \dot{\varepsilon} \cdot \exp(\frac{Q}{RT}) = A\,[\sinh(\alpha\sigma)]^n \tag{9}$$

Taking the natural logarithm of both sides of Eq. (9) gives

$$\ln Z = \ln A + n\ln[\sinh(\alpha\sigma)] \quad (10)$$

It is evident that the values of $\ln A$ and n are the intercept and slope of the line in $\ln Z$-$\ln[\sinh(\alpha\sigma)]$ plot, respectively. With the values of $\ln Z$ and corresponding flow stress at 0.25 strain, the relationship between $\ln Z$ and $\ln[\sinh(\alpha\sigma)]$ can be obtained, as shown in Fig. 4. Then, the values of $\ln A$ and n are 44.794 and 6.891, respectively.

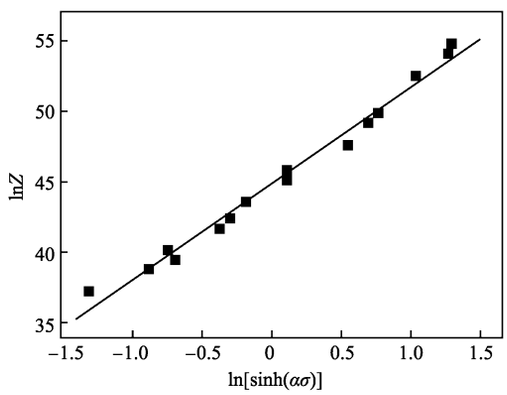

Fig. 4 Relationship between $\ln Z$ and $\ln[\sinh(\alpha\sigma)]$ for the experimental steel

Employing the same solution procedure, the values of α, n, Q, and $\ln A$ were determined at different strains (in the range of 0.05—0.60) at an interval of 0.05. These values were employed to fit the polynomial. The order of the polynomial varied from 2 to 9. Finally, a sixth order polynomial, as shown in Eq. (11), is found to represent the effect of strain on material constants with a very good correlation and generalization (Fig. 5). The coefficients of the polynomial are given in Table 1. Higher order polynomial (higher than 6) is found to over-fit thus losing its ability of true representation and generalization.

$$\begin{cases} \alpha = C_0 + C_1\varepsilon + C_2\varepsilon^2 + C_3\varepsilon^3 + C_4\varepsilon^4 + C_5\varepsilon^5 + C_6\varepsilon^6 \\ n = D_0 + D_1\varepsilon + D_2\varepsilon^2 + D_3\varepsilon^3 + D_4\varepsilon^4 + D_5\varepsilon^5 + D_6\varepsilon^6 \\ Q = E_0 + E_1\varepsilon + E_2\varepsilon^2 + E_3\varepsilon^3 + E_4\varepsilon^4 + E_5\varepsilon^5 + E_6\varepsilon^6 \\ \ln A = F_0 + F_1\varepsilon + F_2\varepsilon^2 + F_3\varepsilon^3 + F_4\varepsilon^4 + F_5\varepsilon^5 + F_6\varepsilon^6 \end{cases} \quad (11)$$

From Eq. (9), following equation can be obtained[20]:

$$\sigma = \frac{1}{\alpha}\sinh^{-1}\left(\frac{Z}{A}\right)^{1/n} \quad (12)$$

After some algebraic operations, then

$$\sigma = \frac{1}{\alpha}\ln\left\{\left(\frac{Z}{A}\right)^{1/n} + \left[\left(\frac{Z}{A}\right)^{2/n} + 1\right]^{1/2}\right\} \quad (13)$$

Therefore, the modified constitutive equation with strain-dependent constants, which can predict the flow stress at a particular strain, can be expressed as follows:

$$\sigma = \frac{1}{\alpha}\ln\left\{\left(\frac{Z}{A}\right)^{1/n} + \left[\left(\frac{Z}{A}\right)^{2/n} + 1\right]^{1/2}\right\}$$

$$Z = \dot{\varepsilon} \cdot \exp\left(\frac{Q}{RT}\right)$$

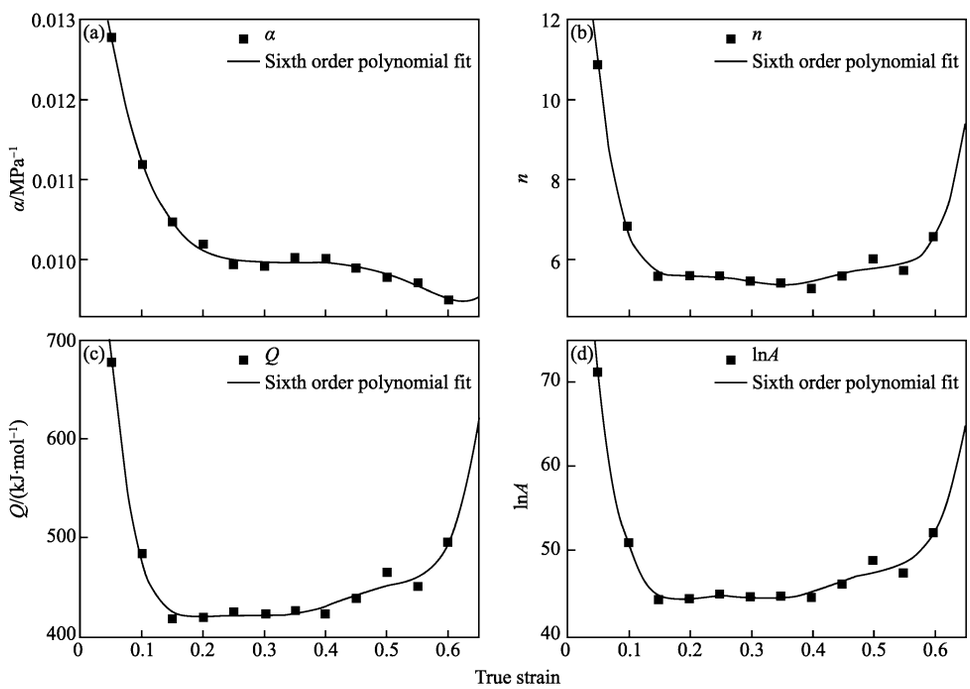

Fig. 5 Relationship between α, n, Q, $\ln A$ and strain by polynomial fit of the experimental steel

Table 1 Coefficients of polynomial for α, n, Q and $\ln A$

α	n	Q	$\ln A$
$C_0=0.016$	$D_0=22.335$	$E_0=1\,225.197$	$F_0=127.385$
$C_1=-0.077$	$D_1=-320.034$	$E_1=-16\,290.079$	$F_1=-1\,679.723$
$C_2=0.437$	$D_2=2\,665.065$	$E_2=131\,901.209$	$F_2=13\,625.990$
$C_3=-1.374$	$D_3=-11\,343.456$	$E_3=-547\,186.612$	$F_3=-56\,632.178$
$C_4=2.557$	$D_4=25\,913.398$	$E_4=1.227\times10^6$	$F_4=127\,055.571$
$C_5=-2.660$	$D_5=-30\,170.429$	$E_5=-1.410\times10^6$	$F_5=-145\,950.883$
$C_6=1.176$	$D_6=14\,058.004$	$E_6=651\,245.336$	$F_6=67\,351.394$

$$\alpha = 0.016 - 0.077\varepsilon + 0.437\varepsilon^2 - 1.374\varepsilon^3 + 2.557\varepsilon^4 - 2.660\varepsilon^5 + 1.176\varepsilon^6$$

$$n = 22.335 - 320.034\varepsilon + 2\,665.065\varepsilon^2 - 11\,343.456\varepsilon^3 + 25\,913.398\varepsilon^4 - 30\,170.429\varepsilon^5 + 14\,058.004\varepsilon^6$$

$$Q = 1\,225.197 - 16\,290.079\varepsilon + 131\,901.209\varepsilon^2 - 547\,186.612\varepsilon^3 + 1.227\times10^6\varepsilon^4 - 1.410\times10^6\varepsilon^5 + 651\,245.336\varepsilon^6$$

$$\ln A = 127.385 - 1\,679.723\varepsilon + 13\,625.990\varepsilon^2 - 56\,632.178\varepsilon^3 + 127\,055.571\varepsilon^4 - 145\,950.883\varepsilon^5 + 67\,351.394\varepsilon^6 \quad (14)$$

On the other hand, the stress at a strain of 0.25 is taken as the peak stress according to the hot deformation behavior of experimental steel. So the original constitutive equation, which does not consider the effect of strain on material constants and can merely predict the peak stress, can be expressed as follows according to Eqs. (1), (2) and (3) and the above calculation of material constants at a true strain of 0.25:

$$\begin{cases} \sigma = \dfrac{1}{0.009\,9}\ln\left\{\left(\dfrac{Z}{2.843\times10^{19}}\right)^{1/6.891} + \left[\left(\dfrac{Z}{2.843\times10^{19}}\right)^{2/6.891}+1\right]^{1/2}\right\} \\ Z = \dot{\varepsilon}\cdot\exp\left(\dfrac{51\,037.682}{T}\right) \end{cases} \quad (15)$$

2.3 Verification of modified constitutive equation

In order to evaluate the predictability of the modified constitutive equation (considering the effect of strain), the comparison between the measured flow stress curves and predicted flow stress values is presented in Fig. 6. It can be observed that the predicted flow stress values obtained from the modified constitutive equation can track the measured flow stress values throughout the deformation conditions except at 800 ℃ in 1 s^{-1} and at 700 ℃ in 5 and 10 s^{-1}.

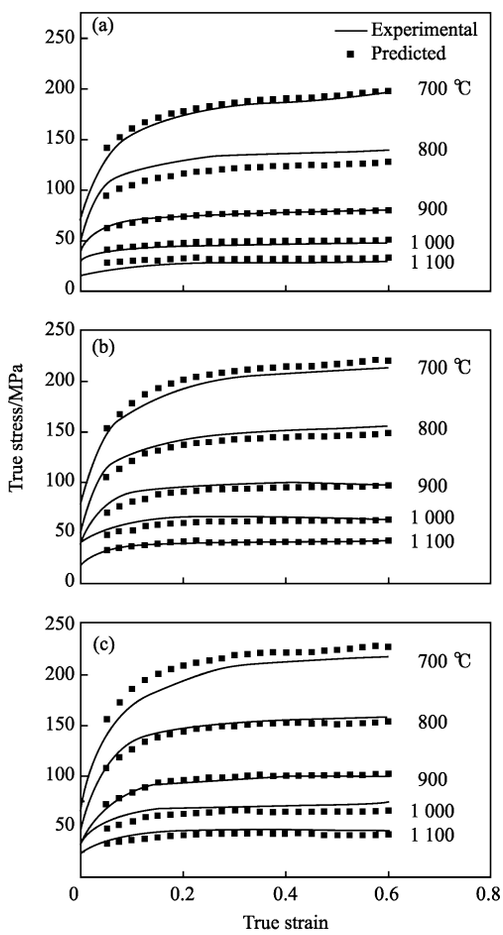

(a) 1 s^{-1}; (b) 5 s^{-1}; (c) 10 s^{-1}.

Fig. 6 Comparison between measured and predicted flow stress from the modified constitutive equation of experimental steel at 700—1 100 ℃ and different strain rates

The reason for losing the predictability of the modified constitutive equation at 800 ℃ in 1 s^{-1} and at 700 ℃ in 5 and 10 s^{-1} is not quite clear. The predicted flow stress values at 800 ℃ in 1 s^{-1} are lower than the measured flow stress values. Studies demonstrated that the increase in the average Taylor

factor (i. e., increase the intensities of the "hard" (deformation) texture components) occurred with increasing the strain in the absence of recrystallization during compression tests. This could cause some amount of hardening (textural hardening) and decreases the probability of plastic deformation[33-35]. According to flow stress curves, on one hand, dynamic recovery (DRV) may be the major softening mechanism during hot deformation. On the other hand, the initial microstructure before deformation and microstructure after deformation at 800 ℃ in 1 s^{-1} were analyzed with EBSD and the Taylor factor of the scanned region was calculated, as shown in Fig. 7. It can be seen that the volume fractions of grains having the Taylor factor of 2—3 and 3—4 are 72.5% and 27.5% before deformation, respectively, while they are 60.3% and 39.7% after deformation at 800 ℃ and 1 s^{-1}, respectively. In other words, the Taylor factor increases after hot deformation in this study. Accordingly, the underestimation in the flow stress prediction at 800 ℃ in 1 s^{-1} occurs. However, the modified constitutive equation can predict the flow stress at other deformation conditions except at 700 ℃ in 5 and 10 s^{-1} even though the increase in the average Taylor factor may have taken place as well. It is possible that the effect of increasing the average Taylor factor during hot deformation on hardening is not so significant since the softening is already high under some deformation conditions such as relatively high temperatures or the thermal softening (the increase in temperature during hot deformation) is already obvious under some deformation conditions such as relatively low temperatures.

The predicted flow stress values at 700 ℃ in 5 and 10 s^{-1} are higher than the measured flow stress values. The temperature rise due to deformation heating at high strain rates (i. e., 10 s^{-1}), which can result in the thermal softening, may be the main reason for this. Because the test time is too short to allow for heat transfer due to the deformation at relatively high strain rates, the specimen temperature rises, leading to the thermal softening[36]. Therefore, the overestimation in flow stress prediction at 700 ℃ in 5 and 10 s^{-1} occurs. However, the modified constitutive equation can predict the flow stress at other temperatures also at high strain rates except at 800 ℃ in 1 s^{-1} even though the deformation heating and subsequent temperature rise maybe take place as well under these deformation conditions. It is possible that the effect of the deformation heating and subsequent temperature rise during hot deformation on softening at these high temperatures is not so significant since available thermal activation energy is already high to induce thermal softening[19]. Further work requires to be done on the changes in the average Taylor factor and deformation heating

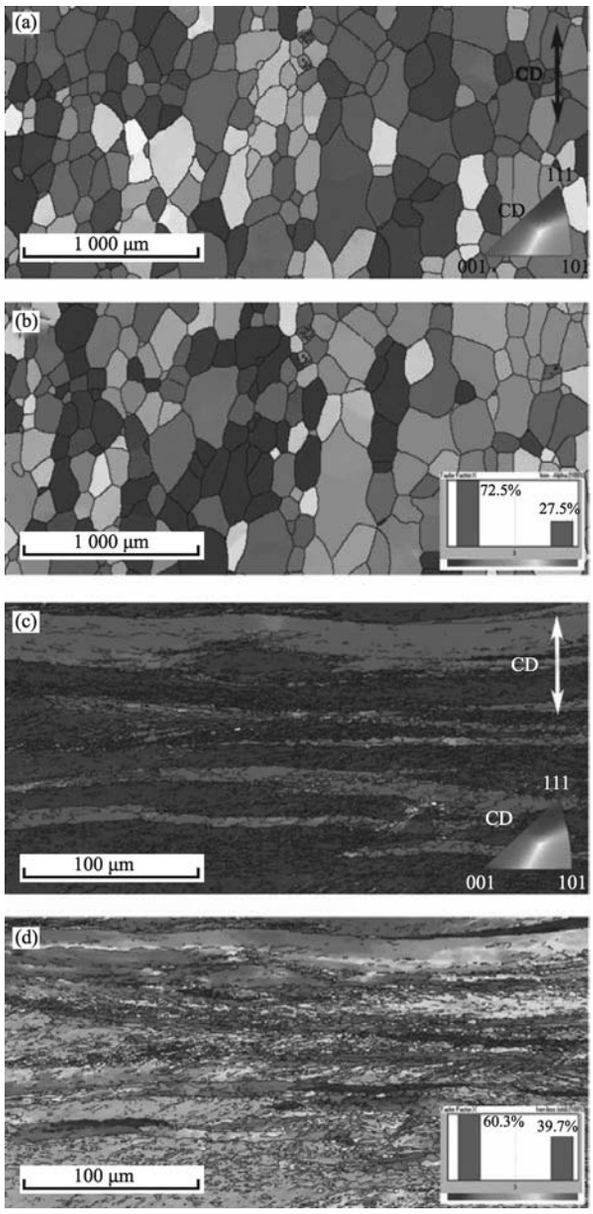

(a) Orientation map of initial microstructure;
(b) Taylor factor map of initial microstructure;
(c) Orientation map of microstructure after deformation at 800 ℃ and 1 s^{-1};
(d) Taylor factor map of microstructure after deformation at 800 ℃ and 1 s^{-1}.
CD denotes compression axis direction.

Fig. 7 Orientation maps and corresponding Taylor factor maps of the initial microstructure before deformation and microstructure after deformation at 800 ℃ in 1 s^{-1}

and there needs to be a systematic study of hardening and softening during hot deformation in order to draw a firm conclusion.

In order to quantitatively evaluate the predictability of the modified constitutive equation, standard statistical parameters such as correlation coefficient R^2 and average absolute relative error AARE were employed. They can be expressed as follows:

$$R^2=\frac{\sum_{i=1}^{N}(M_i-\overline{M})\ (P_i-\overline{P})}{\sqrt{\sum_{i=1}^{N}(M_i-\overline{M})^2\sum_{i=1}^{N}(P_i-\overline{P})^2}} \tag{16}$$

$$\text{AARE}\ (\%)=\frac{1}{N}\sum_{i=1}^{N}\left|\frac{M_i-P_i}{M_i}\right|\times 100 \tag{17}$$

where, M is the measured value; P is the predicted value obtained from the modified constitutive equation; $\overline{M}$ and $\overline{P}$ are the mean values of M and P, respectively; N is the total number of data points. The correlation coefficient provides information on the strength of linear relationship between the measured and predicted values, whereas the average absolute relative error is computed through a term by term comparison of the relative error. For the modified constitutive equation, it can be seen from Fig. 8 that a good correlation is obtained between the measured and predicted flow stress values and the AARE is found to be 5.76%. For the original constitutive equation, it can be seen from Fig. 9 that the correlation between the measured and predicted flow stress values with a correlation coefficient value of 0.989 1 is not better than that for the modified constitutive equation with a correlation coefficient value of 0.994 5 and the AARE is found to be 5.72%. According to these statistical analyses, the modified constitutive equation reveals the better reliability and stability than the original constitutive equation, and the modified constitutive equation with strain-dependent constants can predict the flow stress for a given strain but the original constitutive equation can merely predict the peak stress at deformation temperatures of 700 to 1 100 ℃ and strain rates of 1 to 10 s^{-1} for the ultra purified 17% Cr ferritic stainless steel stabilized with Nb and Ti.

Ferritic stainless steels possess poor formability and surface quality in comparison with austenitic stainless steels, which can be attributed to low r-value, severe surface ridging and sticking phenomenon during hot rolling[1,7]. On one hand, improvement of r-value and ridging resistance for ferritic stainless steels has been attempted by several approaches, such as controlling the chemical composition, solidification structure, thermo-mechanical processing, hot band annealing condition, intermediate annealing between cold rolling, and cold rolling reduction ratio and employing the strip casting and changing the strain path by a unique deformation such as equal channel angular pressing[3-4,6-7]. Many papers have paid attention to increasing the r-value and weakening the ridging resistance for ferritic stainless steels through optimizing the thermo-mechanical processing[4-7]. It was shown that compared to hot rolling at a high finisher entry temperature, hot rolling at a low finisher entry temperature (especially, approximately 700 ℃) was of benefit for the formation of in-grain shear bands in the rolled microstructure, which can provide more nucleation sites for recrystallization grains, enhance the formation of {111} recrystallization textures and increase the r-value of the final sheet. Moreover, due to the rolled microstructure refinement by the

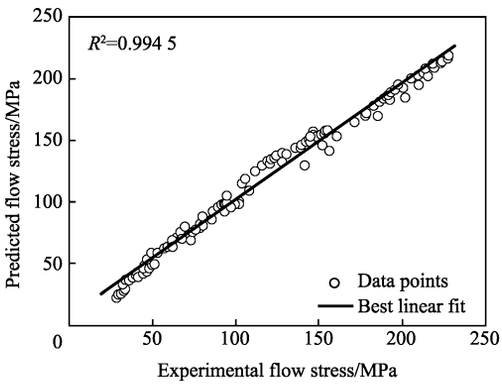

Fig. 8 Correlation between experimental and predicted flow stress values obtained from the modified constitutive equation of experimental steel

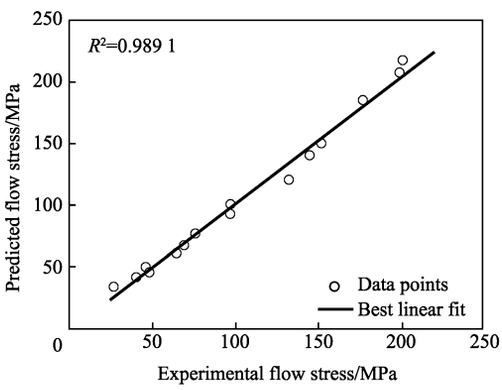

Fig. 9 Correlation between experimental and predicted flow stress values obtained from original constitutive equation of experimental steel

formation of in-grain shear bands, the elongated grains with α-fiber orientations were consumed during hot-band annealing, improving the ridging resistance by eliminating the grain colonies in the final sheet. On the other hand, weakening of the sticking behavior for ultra purified ferritic stainless steels has been attempted by controlling the oxide scale, rolling temperature, strain rate and roughness of the work rolls[5]. It demonstrated that the sticking phenomenon was supposed to be weakened by decreasing the rolling temperature, increasing the strain rate and decreasing the surface roughness of the work rolls.

Therefore, decreasing the rolling temperature is beneficial to increasing the r-value, enhancing the ridging resistance, reducing the sticking and eventually improving the product quality of final sheet for the ferritic stainless steels, and the product quality can be significantly improved when the finisher entry temperature is at 700 ℃. Zhang[37] developed a new hot rolling process which had been verified by pilot rolling experiments and found that compared with the conventional hot rolling process with finish rolling at about 900 ℃, the new hot rolling process with finish rolling at about 700 ℃ has great beneficial effect on minimization of sticking for ultra purified ferritic stainless steel, as shown in Fig. 10. It can be seen that after conventional hot rolling process, there are some surface defects in the hot rolled and annealed bands after pickling along rolling direction which can be ascribed to the sticking behavior during hot rolling (Fig. 10(a))[37]. After new hot rolling process, only minor surface defects were observed in the hot rolled and annealed bands after pickling due to the weakening of the sticking behavior (Fig. 10(b)). He suggested that decrease of rolling temperatures can efficiently increase the deformation resistance of the steel to improve the sticking resistance. Although the flow stress increases with decreasing deformation temperature (Fig. 2), the flow stress of the experimental steel during deformation at 700 ℃ is close to that of the commercial high-strength steel during deformation at 850 ℃[22]. This indicates that the deformation resistance of experimental steel is low during deformation at 700 ℃ and hot rolling at a low finisher entry temperature of 700 ℃ can be achieved in practical production.

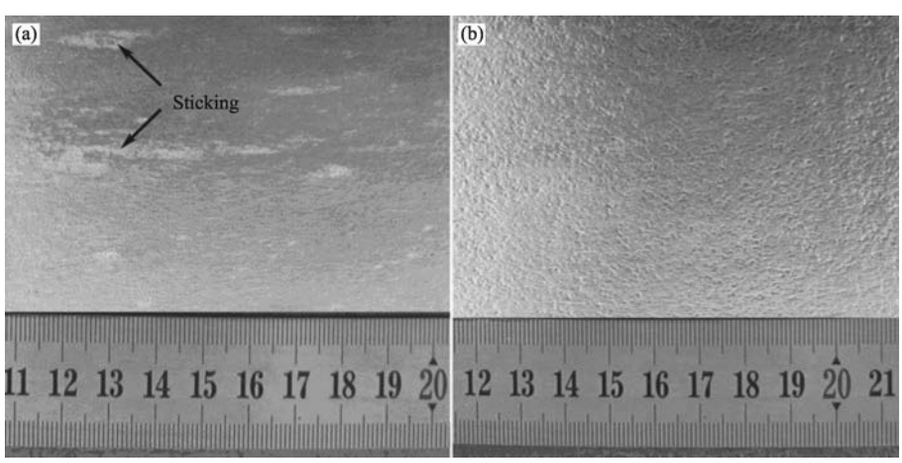

(a) Conventional hot rolling process; (b) New hot rolling process.

Fig. 10 Surface qualities of hot rolled and annealed bands with different hot rolling processes after pickling

3 Conclusions

(1) The effect of strain was incorporated in the constitutive equation by establishing polynomial relationship between the material constants and strain. A sixth-order polynomial was suitable to represent the effect of strain.

(2) The modified constitutive equation describing the flow stress as a function of strain, strain rate and temperature was developed by considering the effect of strain and could very well predict the flow stress throughout the deformation conditions except at 800 ℃ in 1 s^{-1} and at 700 ℃ in 5 and 10 s^{-1}.

(3) Loss of reliability of the modified constitutive equation at 800 ℃ in 1 s^{-1} was possibly explained by the increase in average Taylor factor during hot deformation.

(4) Loss of reliability of the modified constitutive equation at 700 ℃ in 5 and 10 s^{-1} was possibly explained by the increase in temperature during hot deformation.

(5) The optimum window for improving the

product quality of final sheet for the ferritic stainless steels was found to be hot rolling at a low finisher entry temperature of 700 ℃, which can be achieved in practical production.

References:

[1] K. H. Lo, C. H. Shek, J. K. L. Lai, Mater. Sci. Eng. R 65 (2009) 39-104.

[2] S. M. Kim, Y. S. Chun, S. Y. Won, Y. H. Kim, C. S. Lee, Metall. Mater. Trans. A 44 (2013) 1331-1339.

[3] H. T. Liu, Z. Y. Liu, G. D. Wang, ISIJ Int. 49 (2009) 890-896.

[4] C. Zhang, Z. Y. Liu, G. D. Wang, J. Mater. Process. Technol. 211 (2011) 1051-1059.

[5] C. Zhang, Z. Y. Liu, Y. Xu, G. D. Wang, J. Mater. Process. Technol. 212 (2012) 2183-2192.

[6] F. Gao, Z. Y. Liu, H. T. Liu, G. D. Wang, Acta Metall. Sin. (Engl. Lett.) 24 (2011) 343-350.

[7] F. Gao, Z. Y. Liu, H. T. Liu, G. D. Wang, Mater. Charact. 75 (2013) 93-100.

[8] T. Sawatani, K. Shimizu, T. Nakayama, M. Miyoshi, Tetsu-to-Hagane 63 (1977) 843-854.

[9] Y. Uematsu, K. Yamazaki, Tetsu-to-Hagane 78 (1992) 632-639.

[10] W. Jin, J. Y. Choi, Y. Y. Lee, ISIJ Int. 38 (1998) 739-743.

[11] W. Jin, J. Y. Choi, Y. Y. Lee, ISIJ Int. 40 (2000) 789-793.

[12] D. J. Ha, C. Y. Son, J. W. Park, J. S. Lee, Y. D. Lee, S. Lee, Mater. Sci. Eng. A 492 (2010) 49-59.

[13] J. Zhou, J. B. Zhang, G. S. Ji, D. Fan, Trans. Mater. Heat Treat. 31 (2010) No. 9, 50-54.

[14] L. H. Yang, L. J. Li, Y. Z. Liu, L. Y. Zhou, Heat Treat. Met. 36 (2011) No. 12, 78-81.

[15] F. Gao, Z. Y. Liu, G. D. Wang, J. Northeast. Univ. Nat. Sci. 32 (2011) 1406-1409.

[16] C. Zhang, Z. Y. Liu, G. D. Wang, J. Iron Steel Res. 22 (2010) No. 12, 27-32.

[17] F. A. Slooff, J. Zhou, J. Duszczyk, L. Katgerman, Scripta Mater. 57 (2007) 759-762.

[18] F. A. Slooff, J. Zhou, J. Duszczyk, L. Katgerman, J. Mater. Sci. 43 (2008) 7165-7170.

[19] S. Mandal, V. Rakesh, P. V. Sivaprasad, S. Venugopal, K. V. Kasiviswanathan, Mater. Sci. Eng. A 500 (2009) 114-121.

[20] H. Mirzadeh, J. M. Cabrera, A. Najafizadeh, Metall. Mater. Trans. A 43 (2012) 108-123.

[21] Y. C. Lin, M. S. Chen, J. Zhong, Comput. Mater. Sci. 42 (2008) 470-477.

[22] Y. C. Lin, M. S. Chen, J. Zhong, Mater. Sci. Eng. A 499 (2009) 88-92.

[23] X. P. Liang, Y. Liu, H. Z. Li, C. X. Zhou, G. F. Xu, Mater. Des. 37 (2012) 40-47.

[24] A. Etaati, K. Dehghani, G. R. Ebrahimi, H. Wang, Met. Mater. Int. 19 (2013) No. 1, 5-9.

[25] F. Gao, Y. R. Xu, B. Y. Song, K. Xia, Metall. Mater. Trans. A 31 (2000) 21-27.

[26] J. H. Zhou, K. Z. Guan, The Resistance to Plastic Deformation of Metals, China Machine Press, Beijing, 1989.

[27] J. H. Zhou, K. Z. Guan, Acta Metall. Sin. 22 (1986) No. 1, B31-B39.

[28] C. M. Sellars, W. J. McTegart, Acta Metall. 14 (1966) 1136-1138.

[29] Y. Wang, D. L. Lin, J. Mater. Sci. Lett. 19 (2000) 1185-1188.

[30] S. Banerjee, P. S. Robi, A. Srinivasan, L. Praveen Kumar, Mater. Sci. Eng. A 527 (2012) 2498-2503.

[31] X. D. Huang, H. Zhang, Y. Han, W. X. Wu, J. H. Chen, Mater. Sci. Eng. A 527 (2010) 485-490.

[32] C. Zener, J. H. Hollomon, J. Appl. Phys. 15 (1944) 22-32.

[33] M. E. Kassner, M. Z. Wang, M. T. Perez-prado, S. Alhajeri, Metall. Mater. Trans. A 33 (2002) 3145-3153.

[34] G. J. Baczynski, J. J. Jonas, L. E. Collins, Metall. Mater. Trans. A 30 (1999) 3045-3054.

[35] D. Samantaray, C. Phaniraj, S. Mandal, A. K. Bhaduri, Mater. Sci. Eng. A 528 (2011) 1071-1077.

[36] Y. C. Lin, M. S. Chen, J. Zhong, Mech. Res. Commun. 35 (2008) 142-150.

[37] C. Zhang, Sticking Mechanism in Hot Strip Rolling and Control of Microstructure and Texture for Ultra Purified 21%Cr Ferritic Stainless Steel, Northeastern University, Shenyang, 2011, 115-125.